Chapter

Thermal Evolution of Geopolymer in the Process of High-Temperature Treatment

Jingkun Yuan, Peigang He and Dechang Jia

Abstract

More and more attention had been given to geopolymers (GPs) over the last decades because of an increasing urgency to search for high-performance and/or environment-friendly alternatives to traditional Portland cement. In addition, geopolymer technology could also provide an innovative approach to prepare advanced ceramic products by overcoming problems faced in the conventional preparation technology. With only the need to go through appropriate thermal treatment procedure, geopolymers could be directly in situ transformed into advanced ceramics such as leucite or pollucite with adjustable microstructures, mechanical properties, coefficient of thermal expansion, and melting points. In the process of high-temperature treatment, multiple parameters, such as the composition of geopolymer, treatment temperature, thermal insulation, etc., would affect the phase composition and microstructure of the resulting products. In the present chapter, two kinds of mixed-alkali metal ion-activated geopolymer systems, $Cs_{(1-x)}Li_xGP$ (where x = 0, 0.1, 0.2, and 0.3) and $Cs_{(1-x)}Na_xGP$ (where x = 0, 0.1, 0.2, 0.3, and 0.4), respectively, were designed and prepared. Phase composition, microstructure evolution, and thermal expansion behaviors of the ceramics derived from the geopolymers were characterized and the effects of ion substitution on the thermal evolution of geopolymer were evaluated.

Keywords: geopolymer, high-temperature treatment, pollucite, spodumene, amorphous glass phase, phase composition, microstructure, thermal expansion behavior

1. Introduction

More and more attention had been given to geopolymers over the last decades because of an increasing urgency to search for high-performance and/or environment-friendly alternatives to traditional Portland cement [1–6]. They were typically synthesized at ambient or elevated temperature by alkali-activated process between alkali-activated solutions and aluminosilicates. And the source of aluminosilicates was very extensive and inexpensive, such as metakaolin, fly ash, blast furnace slag, etc. [7–11]. Most notably, there was almost no emission of greenhouse gases throughout the preparation process, which made geopolymer technology more competitive in terms of environmental and economic advantages.

From their composition, geopolymers were a class of amorphous materials consisting of cross-linked $[AlO_4]^-$ and $[SiO_4]$ tetrahedra units, and the negative charge aluminum in fourfold coordination was balanced by alkali metal

or alkaline earth metal cation, such as Na^+, K^+, Mg^{2+}, and Ca^{2+} [12–15]. As for geopolymers, alkali metal hydroxides were involved in many processes during the alkali-activated reaction or geopolymerization reaction, including accelerating the dissolution of aluminosilicates, stabilizing the solution species and colloids, reducing the electrostatic repulsion between the anions, and promoting gel formation and rearrangement [16–18]. Therefore, as for alkali metal hydroxide, the OH^- group in it mainly accounted for creating the reactive precursors, while the alkali cations would play an important role in catalyzing gel formation, acting as a structure-directing agent. Since the alkali metal was one of the most easily alterable constituents in the framework of geopolymer, it was very valuable to investigate the effects of alkali cation species on the evolution of microstructure and properties of the geopolymer system [19]. Fernández-Jiménez et al. proved that Na^+ was much more conducive to the coagulation and precipitation process than K^+, and the resulting geopolymer gels would consist of a much wider diversity of Q^n species in the case of Na^+ [20–22]. Duxson et al. suggested that larger cations were more inclined to bind by the gel in mixed-alkali-activated systems that contained Na^+ and K^+ [23]. Ikuo et al. reported that the thermal expansion coefficient (CTE) of the cubic cesium leucite-based compounds decreased with much smaller ions occupying/substituting the crystallographic sites of Cs^+, such as Na^+ or Li^+ substitutional ions [24–26].

Pollucite ($CsAlSi_2O_6$) exhibits a unique thermal expansion curve that has two stages: the average CTE is ~12.5×10^{-6} K^{-1} from 298 to 473 K and ~2.2×10^{-6} K^{-1} from 473 to 1473 K [24, 27]. In recent years, many reports have given evidence that the thermal expansion of pollucite decreased with ionic substitution at the Cs^+ sites by smaller alkali metal ions, such as Na^+ and Li^+ [24–33]. But, the mechanisms about how thermal expansion properties of pollucite are affected have not yet been studied clearly. In general, there were three main methods to prepare pollucite, including the solid-state reaction method, sol-gel method, and ion exchange method from leucite [34]. However, solid-state reaction always required high sintering temperatures and easily suffered from problems of cesium volatilization, agglomeration, furnace contamination, etc. Ion exchange and sol-gel techniques were also uncompetitive due to their high cost and severe preparation conditions. Moreover, it was almost impossible to get fully densified pollucite ceramic products because the volatilization of cesium was inevitable in the high-temperature environment during its preparation process. Therefore, only limited researches have been made on pollucite glass ceramic until now. In contrast, geopolymer technology could be an excellent alternative to prepare pollucite ceramic products through in situ conversion due to its ability to from crystalline ceramic phase after proper thermal treatment [35].

Therefore, as a part of our continuing research, a series of ion-substituted cesium-based geopolymer samples, $Cs_{(1-x)}Li_xGP$ (where x = 0, 0.1, 0.2, and 0.3) and $Cs_{(1-x)}Na_xGP$ (where x = 0, 0.1, 0.2, 0.3, and 0.4), were prepared. Phase composition, microstructure evolution, and thermal expansion behavior of ceramics derived from $Cs_{(1-x)}Li_xGP$ and $Cs_{(1-x)}Na_xGP$ were characterized, with the aim of investigating the effect of ion substitution on the thermal evolution of the geopolymer.

2. Experiments and characterization

Simultaneous thermogravimetry (TG) and differential thermal analysis (DTA) (Netzsch STA 409, Germany) were carried out under Ar gas flow (20 mL/min) with temperature up to 1200°C at a heating rate of 5°C/min in alumina crucibles. Sample

powders were sintered without the occurrence of any reaction between the samples and the crucible.

The phase composition of samples was analyzed using X-ray diffraction (XRD, 40 KV/100 mA, D/max-γB CuKa, Rigaku Corp., Japan) method to obtain the X-ray diffraction spectra at 2θ = 10°–90° with a scanning speed of 4°/min. Slow step-scans with a step width of 0.02 and a step time of 3 s were carried out to determine the shifts of X-ray spectrum.

The microstructure of geopolymers before and after heat treatment was investigated by a scanning electron microscope (SEM, 30 KV, Helios Nanolab600i, FEI Co., USA). Energy dispersive spectrometer (EDS) was also adopted to study the elemental arrangement and phase distribution. Transmission electron microscope (TEM, 300 KV, Talos, FEI Company) was also employed to analyze its microstructure. For ceramics derived from geopolymer, TEM samples were ion-milled at low temperature, using a Fischione ion mill (Model 2; Export, PA).

3. Results and discussions

3.1 Thermal analysis

Figure 1 displays the results of thermogravimetry (TG) analysis as to $Cs_{(1-x)}Li_xGP$ and $Cs_{(1-x)}Na_xGP$ systems, respectively. Both systems showed similar TG curves. There was significant mass loss as the temperature increased until 800°C. The escape of free water, including water adsorbed on the surface and pore solution, accounted for the mass loss in the interval below 300°C. The mass loss between 300 and 800°C could be mainly attributed to the condensation and polymerization of hydroxyl connected with Si/Al atom, which resulted in the formation of oxo-bridge in the framework of geopolymer [13, 36]. As the temperature rose further, the TG curves remained essentially unchanged, suggesting almost no mass loss in this stage. The total mass loss increased regularly with the increase of Li^+/Na^+ content. Take $Cs_{(1-x)}Na_xGPs$ for example, Na^+ had a smaller ionic radius than that of Cs^+, which means Na^+ ion had a higher hydration energy than that of Cs^+ ion [37]. Therefore, the amount of hydration water associated with Na^+ was much more than that with Cs^+ ion and, so, it was easy to see why the mass losses increased with increase in Na^+ ion substitution amount in the $Cs_{(1-x)}Na_xGP$ system.

Figure 2 displays thermal shrinkage curves of these two geopolymer systems. The process of thermal shrinkage could be divided into four stages [14, 38, 39]: (I) Structural resilience (RT ~100°C): due to only free water lost in this interval, the

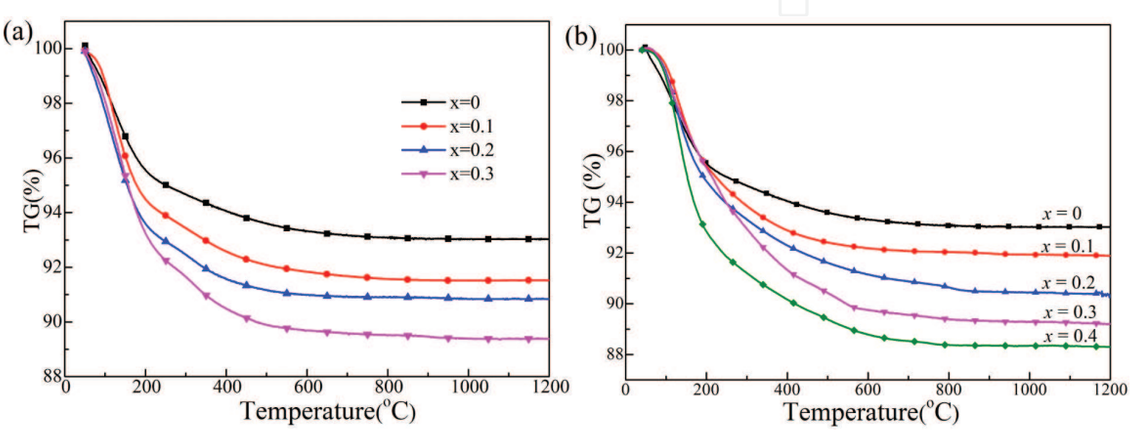

Figure 1.
Thermal gravimetric curves of $Cs_{(1-x)}Li_xGPs$ (a) and $Cs_{(1-x)}Na_xGPs$ (b).

dimensions of the tested samples could be maintained substantially, and the corresponding densification degree of the tested samples did not change significantly synchronously; (II) Dehydration (100–300°C): the causes of the shrinkage and deformation in this interval could be attributed to the capillary contraction induced by the escape of water from micro- and nano-pore solutions; (III) Dehydroxylation (300–800°C): the condensation and polymerization between *T*–OH groups (*T* = Al/Si) caused the water escape and shrinkage in the interval, with more weight damage and shrinkage at this stage than those in stage (II); (IV) Viscous sintering (above 800°C): the shrinkage in this stage was caused by the generation of molten amorphous glass phase, and the presence of molten amorphous glass phase would facilitate sintering and densification, which also means the maximum shrinkage behavior would occur in this stage [13, 19, 40, 41]. When the treatment temperature climbed to 1200°C, almost no shrinkage was observed, suggesting that the shrinkage process was fully completed.

However, after Cs^+ ion was substituted, significant differences are observed in Stage IV. For $Cs_{(1-x)}Li_xGP$ samples, they all showed two sintering steps in Stage IV. Taking $Cs_{0.9}Li_{0.1}GP$ for example, as depicted in **Figure 3**, there were two sintering steps: Region i: 850–1050°C and Region ii: 1050–1300°C. On raising Li^+ ion content from 0 to 30 mol%, the onset temperature of two steps decreased gradually, from 850 to 730°C for Region i and from 1050 to 970°C for Region ii, respectively. In general, the melting points of the $MAlSi_2O_6$ decline with decreasing ionic radius of M^+ ion (M = Li, Na, K, Cs). Meanwhile, onset sintering temperatures for NaGP, KGP, and CsGP were 650°C [36], 850°C [14], and 1200°C [13], respectively, indicating that geopolymer containing M+ ion (MGP) also showed a similar trend with $MAlSi_2O_6$. Therefore, it was reasonable to deduce that LiGP would exhibit the lowest onset sintering temperature, resulting in the lower temperature in Region i of Stage IV. Region ii might be due to melting of Li-based aluminosilicates. It should be pointed out that after doping with Li, all the samples show lower overall thermal shrinkage than pure CsGP, implying that the presence of Li facilitated sintering of $Cs_{(1-x)}Li_xGPs$ to dense microstructure. The same trend could also be observed in the $Cs_{(1-x)}Na_xGP$ system.

3.2 Phase composition

Figure 4 provides XRD patterns of $Cs_{(1-x)}Li_xGPs$ and corresponding ceramic products derived from it. For $Cs_{(1-x)}Li_xGPs$, all the samples show a typical amorphous character with a broad amorphous hump from 20° to 30° 2θ, and almost no changes in phase composition had been observed based the XRD results of $Cs_{(1-x)}Li_xGPs$ with different Li^+ content. However, a substantial amount of pollucite was observed after

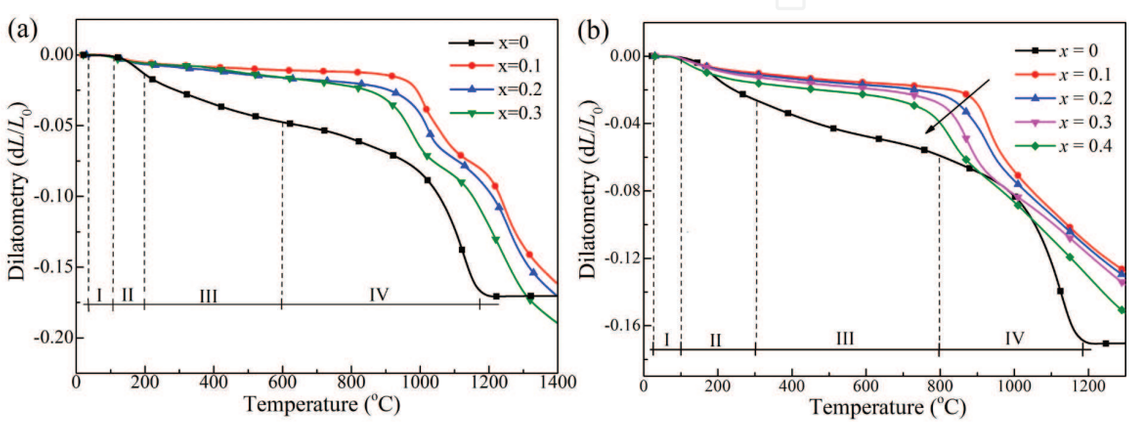

Figure 2.
Thermal shrinkage curves of $Cs_{(1-x)}Li_xGPs$ (a) and $Cs_{(1-x)}Na_xGPs$ (b).

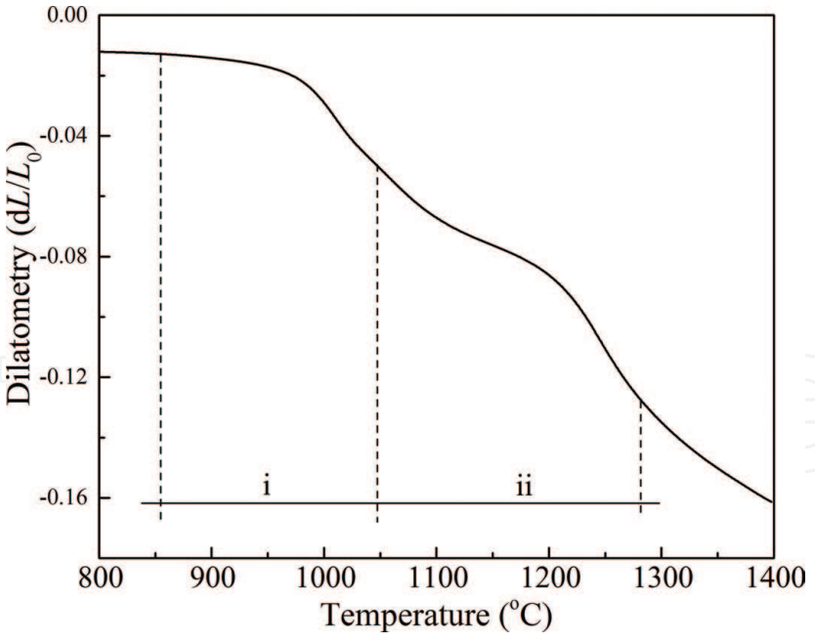

Figure 3.
Partial thermal shrinkage curves of $Cs_{0.9}Li_{0.1}GP$.

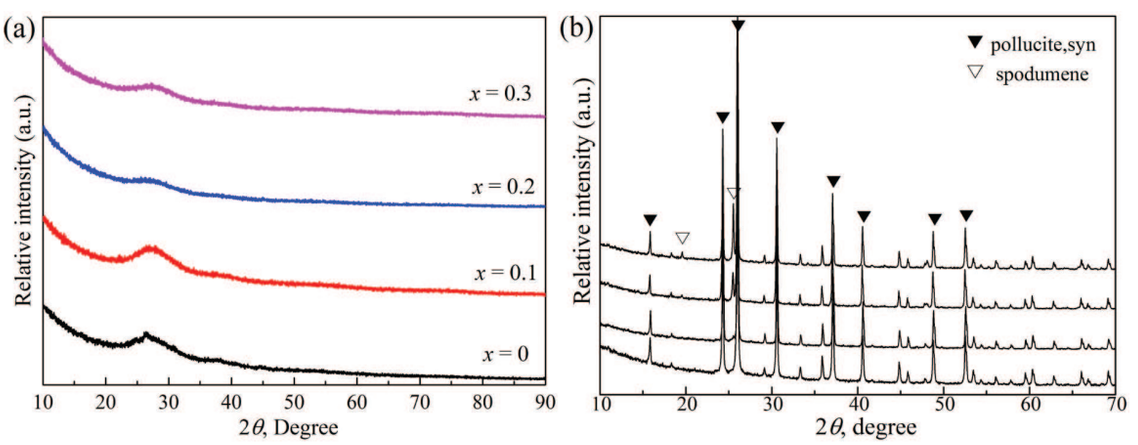

Figure 4.
XRD patterns of $Cs_{(1-x)}Li_xGPs$ (a) and ceramics derived from it (b).

pure CsGP was treated at 1300°C for 2 h. In addition, a small amount of spodumene was also observed after Cs^+ ion was partially substituted by Li^+ ion, and the content of spodumene was proportional to the Li^+ ion substitution in $Cs_{(1-x)}Li_xGPs$ system. The results of quantitative analysis indicated that the content of spodumene was 8.8 and 14.2 wt.% corresponding to $x = 0.2$ and 0.3 in $Cs_{(1-x)}Li_xGPs$ system, respectively. However, the spodumene content was too small to calculate using XRD data when Li^+ ion content was 10 mol%.

Unlike $Cs_{(1-x)}Li_xGPs$ ($x > 0$), the phase composition of $Cs_{(1-x)}Na_xGPs$ ($x > 0$) was not completely amorphous after the introduction of Na^+ ion, and the crystallinity of $Cs_{(1-x)}Na_xGPs$ gradually increased as more Cs^+ ion was substituted. The XRD results indicated the presence of pollucite in the unheated samples partially substituted by Na^+ ion (**Figure 5a**), which suggested that the presence of Na^+ ion would have contributed to the crystallization of pollucite. As for the crystallization of pollucite, a possible reason could be attributed to the formation of a zeolite containing sodium, aluminum, and silicon, such as analcime ($NaAlSi_2O_6{\cdot}H_2O$). The crystallization temperature of zeolite was very low, about 300°C, and the crystallization temperature will become lower (~120°C) for the samples with low Si/Al

ratio under the hydrothermal condition [42, 43]. The geopolymer was nanoporous together with numerous capillaries, filled with pore solution. This structure was like a hydrothermal reaction environment. So, it was possible to produce some fine zeolite nucleus if the reaction time was long enough, although the reaction temperature was low. Analcime and pollucite have similar crystal structure and both were tetragonal and belong to I41/acd (space group). Meanwhile, lattice constant of analcime was a~13.727 and c~13.686, which was close to that of pollucite, a~13.677 and c~13.691 Å. Therefore, it was highly possible that the zeolite nucleus could have served as the nucleation site for pollucite, which contributed to pollucite formation. So, crystalline pollucite could be present in $Cs_{(1-x)}Na_xGPs$ when $x > 0$, which was not the same as the phenomenon of $Cs_{(1-x)}Li_xGPs$ system.

For the resulting ceramics derived from $Cs_{(1-x)}Na_xGPs$ ($x > 0$), only crystalline phases of pollucite were observed in the corresponding XRD pattern, which were different with the $Cs_{(1-x)}Li_xGPs$ system. So, the difference between $Cs_{(1-x)}Li_xGPs$ and $Cs_{(1-x)}Na_xGPs$ also indicated that Na^+ may have only existed in the form of amorphous glass phase.

Based on the result of slow step-scans of ceramics derived from $Cs_{(1-x)}Li_xGPs$, it was possible to find that with increase in Li^+ ion substitution, almost no deviation occurred for the characteristic peaks (4 0 0) and (3 2 1) corresponding to pollucite (**Figure 6**), which proved that the lattice parameters of pollucite did not change as more and more Li^+ ions were introduced [33, 44]. This implied that Li^+ ions did not occupy Cs crystallographic sites of the pollucite framework and phase separation occurred during heating. Diphasic compositions of product ceramics derived from $Cs_{(1-x)}Li_xGPs$ also conform to the aforementioned two-step sintering behavior observed in thermal shrinkage results.

In contrast, for the heated samples derived from $Cs_{(1-x)}Na_xGPs$, the peaks (4 0 0) corresponding to pollucite shifted to the high-angle region with increase in sodium substitution (**Figure 7**), which suggested that the lattice parameters of pollucite decreased with increases in sodium content [33, 44]. The decline of pollucite's lattice parameters proved that Na^+ partially occupied/substituted the crystallographic sites of Cs^+ in the pollucite crystal structure during high-temperature processing. The difference between $Cs_{(1-x)}Na_xGP$ and $Cs_{(1-x)}Li_xGP$ systems could be attributed to the difference between the size of the ions and the form of the substituted ions. Compared with Li^+ ion, the size of Na^+ ion was closer to that of Cs^+ ion. In the $Cs_{(1-x)}Li_x$ system, Li^+ ion was only in the form of spodumene in the heated samples. The different forms of Na^+ and Li^+ ions also suggested that the Na^+ ion had a higher degree of freedom

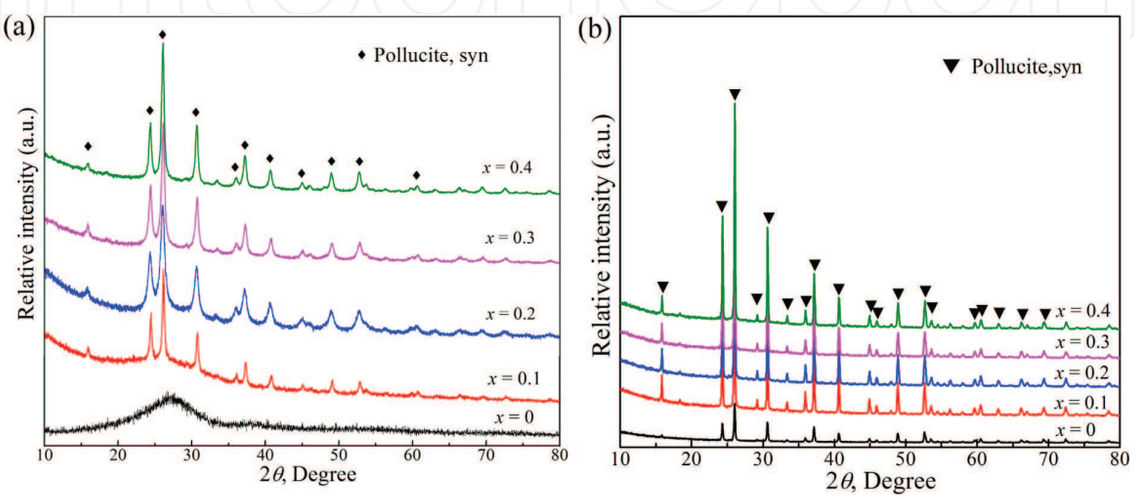

Figure 5.
XRD patterns of $Cs_{(1-x)}Na_xGPs$ (a) and ceramics derived from it (b).

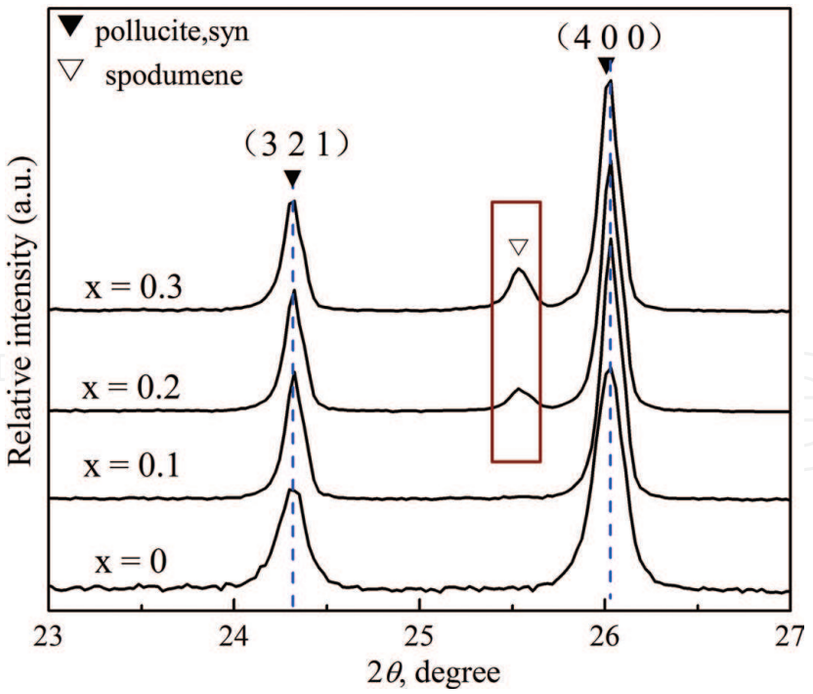

Figure 6.
Slow step-scan XRD patterns of ceramics derived from $Cs_{(1-x)}Li_xGPs$.

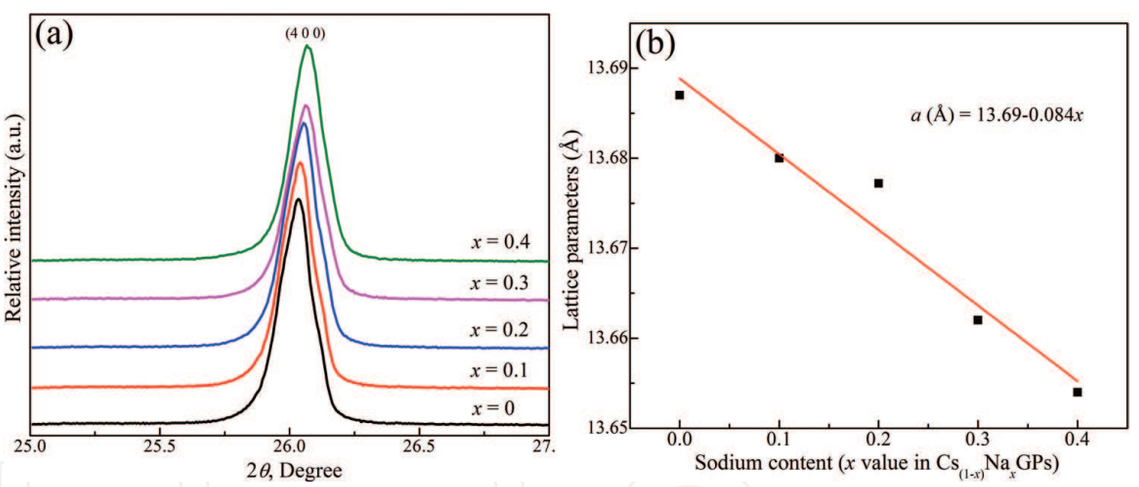

Figure 7.
(a) The (4 0 0) peak in a 2θ of 25–27 (b) Lattice parameters of pollucite.

than Li^+ ion in the mass transfer process. So, it was much easier to occupy/substitute the crystallographic sites of Cs^+ ion in the pollucite crystal structure with Na^+ ion.

3.3 Microstructure evolution

Figure 8 displays the microstructure of as prepared $Cs_{(1-x)}Li_xGPs$. The particles are too small to be observed clearly for pure CsGP. For other $Cs_{(1-x)}Li_xGPs$ ($x \geq 0.1$), the average particle sizes (APSs) are close to ~120, ~200, and ~250 nm corresponding to x = 0.1, 0.2, and 0.3, respectively, which could also be attributed to the difference in hydration energy between Li^+ ion and Cs^+ ions. By comparison, the hydration energy of Li^+ was higher than that of Cs^+, which means that there were more $[AlO_4]$ and $[SiO_4]$ associated with Li^+ ion than that around Cs^+ ion in the framework of the geopolymer. Therefore, higher Li^+ ion contents in the geopolymer always resulted in particles with larger APSs [37]. The same variation trend was also observed in $Cs_{(1-x)}Na_xGPs$ system, as shown in **Figure 9**.

As for $Cs_{(1-x)}Li_xGPs$ system, as shown in **Figure 10**, these precipitates coarsened substantially and all the geopolymers developed a smooth, glassy texture after heating to 1300°C. The coarsening was consistent with the considerable shrinkage observed over the sintering temperature range [45]. Closed pore formations were also observed coincident with significant coarsening and surface area reduction. Pollucite crystals could not be directly observed on any of the fracture surfaces of pure CsGP ceramics despite their noticeable presence in the XRD. As for other $Cs_{(1-x)}Li_xGPs$ ($x \geq 0.1$), the corresponding ceramic product derived from it contain large numbers of spherical particles surrounded by a glassy matrix, with the size of coarsening increasing with Li^+ ion content. The mean diameters of spherical particles were close to ~100 (x = 0.1), ~250 (x = 0.2), and ~400 nm (x = 0.3), respectively. The back-scattered electron (BSE) image suggested the presence of diphasic compositions in corresponding ceramic products derived from $Cs_{(1-x)}Li_xGPs$ ($x \geq 0.1$) (**Figure 10e**). EDS spectra showed that cesium content at point A (**Figure 10f**) was much higher than that at point B (**Figure 10g**). Because EDS was a semi-quantitative analytical measure and Li^+ ion could not be detected by it, so, the results of EDS suggested that spherical particle (point A) and glassy matrix (point B) corresponded to pollucite and spodumene, respectively.

From the fracture morphology after hydrofluoric acid (HF) corrosion, the existence of pollucite grains could be clearly observed in ceramic derived from pure GsGP (**Figure 11a**). In contrast, a polydisperse distribution of pollucite crystals and pores left after dissolution of molten glass phase during etching after the introduction of Cs^+ ion, and the coarsening trend of pollucite grains were also obvious (**Figure 11**).

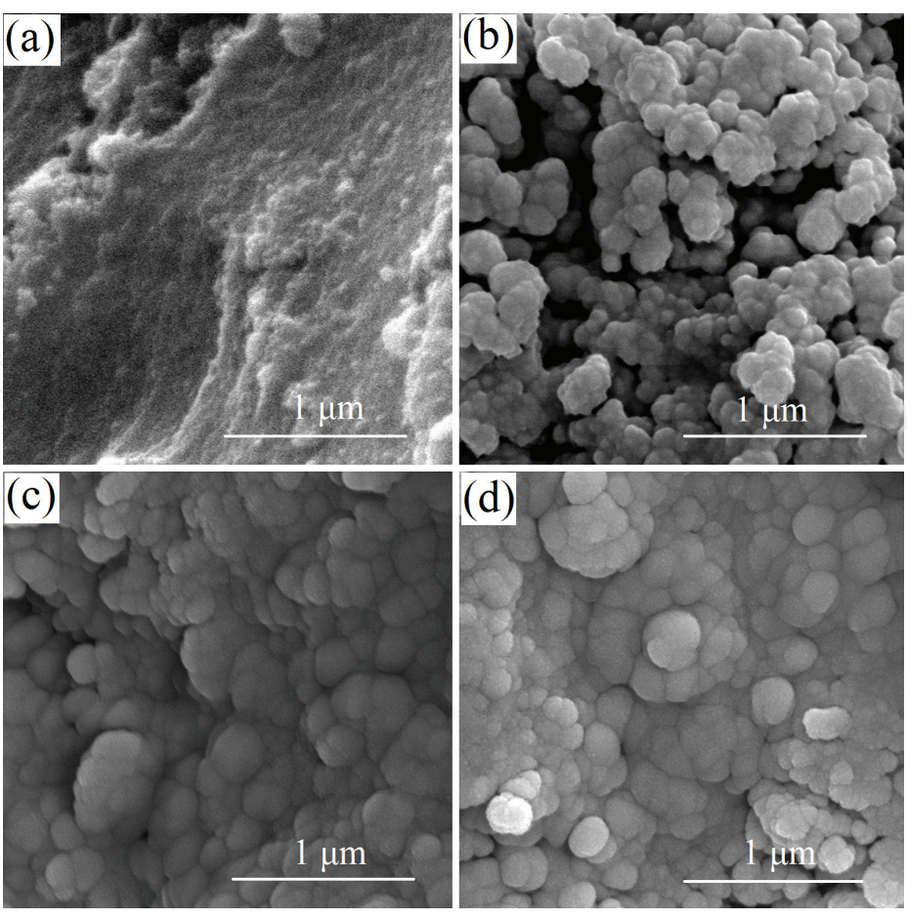

Figure 8.
Microstructure of $Cs_{(1-x)}Li_xGPs$, (a) x = 0, (b) x = 0.1, (c) x = 0.2, (d) x = 0.3 (observed from fracture surface).

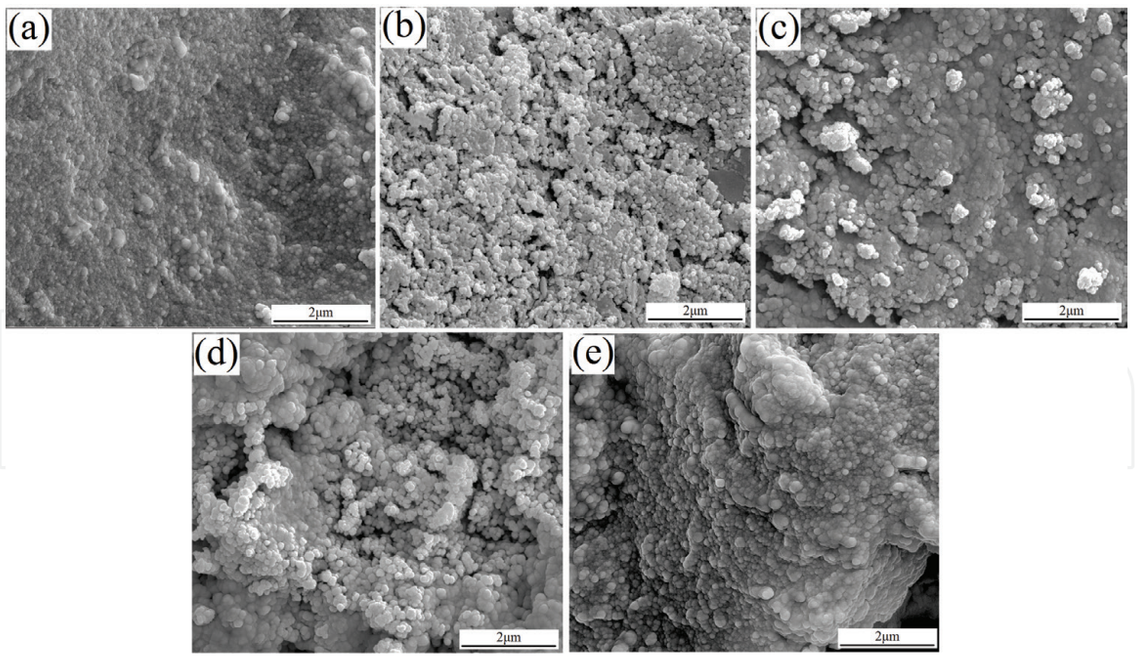

Figure 9.
Microstructure of $Cs_{(1-x)}Na_xGPs$, (a) x = 0, (b) x = 0.1, (c) x = 0.2, (d) x = 0.3, (e) x = 0.4 (observed from fracture surface).

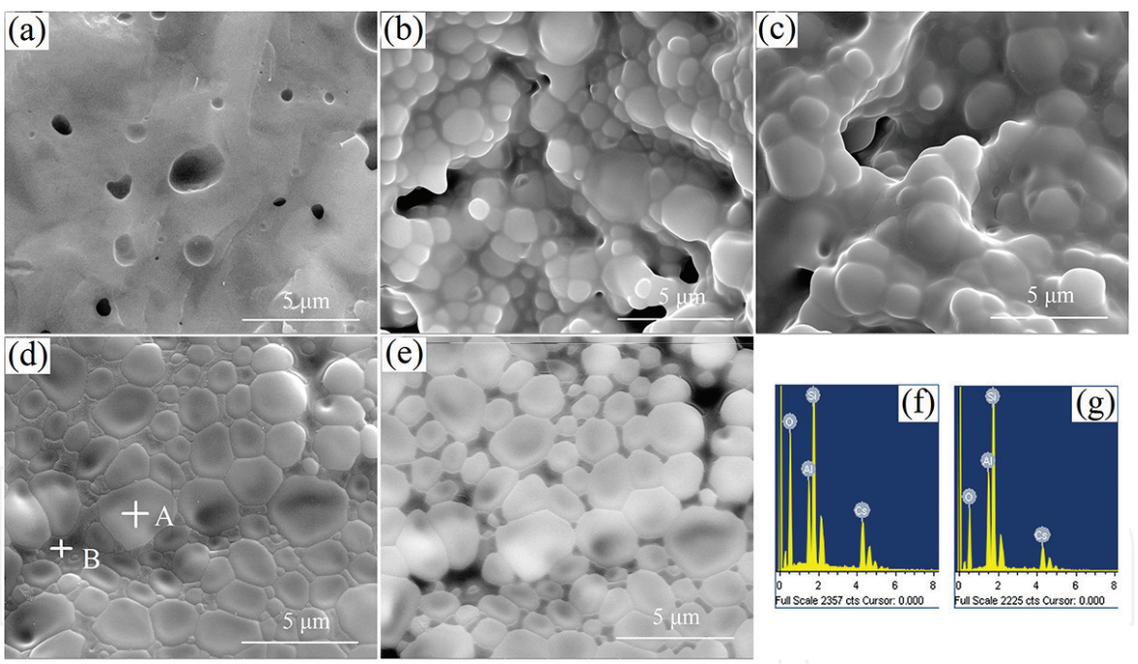

Figure 10.
Microstructure of ceramics derived from $Cs_{(1-x)}Li_xGPs$, (a) x = 0, (b) x = 0.1, (c) x = 0.2, (d) x = 0.3, (e) BSE image of (d), (f) EDS spectrum of point A, (g) EDS spectrum of point B.

Figure 12 shows TEM analysis of the ceramic derived from $Cs_{0.7}Li_{0.3}GP$. The grain boundaries could be observed clearly, and the selected area electron diffraction (SAED) patterns of area A indicate the existence of spodumene crystallite in the resulting products, which may have arisen from the recrystallization of molten spodumene during cooling. Meanwhile, SAED patterns of area B also proved the corresponding grain should be pollucite, and the spodumene phase, with no fixed shape, mainly distributed among pollucite grains or in the grain junction area.

The microstructure morphologies of ceramic products derived from $Cs_{(1-x)}Na_xGPs$ are given in **Figure 13**. By comparison, the particles coarsened significantly after

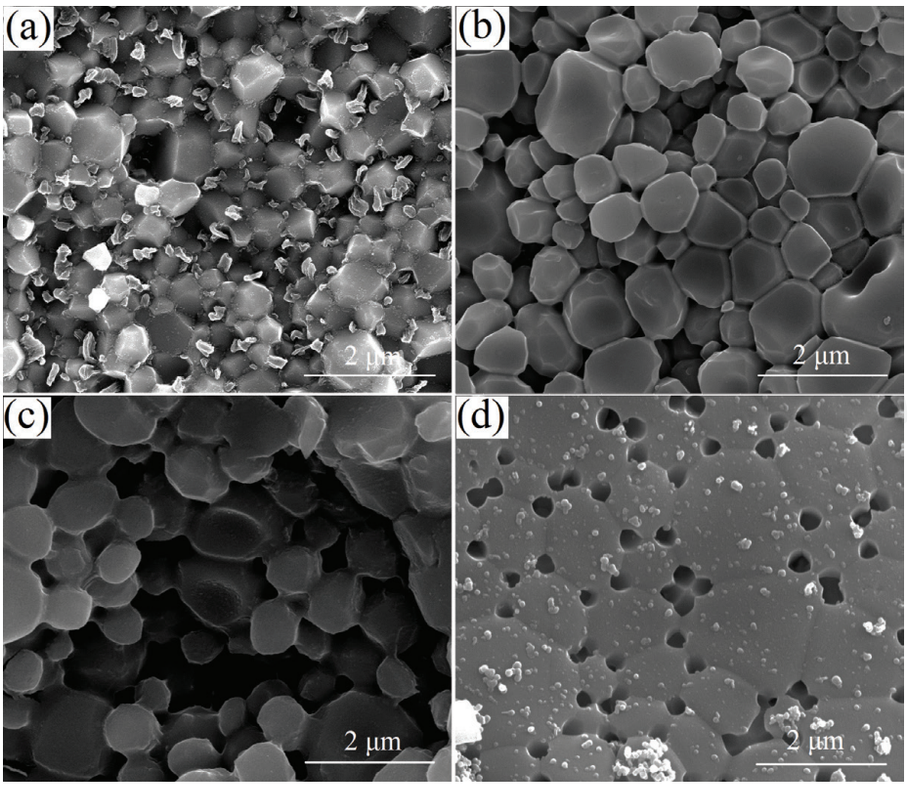

Figure 11.
Microstructure of ceramics derived from $Cs_{(1-x)}Li_xGPs$, (a) x = 0, (b) x = 0.1, (c) x = 0.2, (d) x = 0.3 etched in 4 wt% HF at room temperature for 20 s.

being treated at 1300°C than that of corresponding unheated $Cs_{(1-x)}Na_xGP$ samples. It could be observed that the surface of pollucite grains was covered by smooth and glassy texture. The presence of amorphous glass phase would be conducive to the densification of resulting ceramic products [45].

After etching the samples in 4 wt% HF acid for 20 s, pollucite crystals could be clearly observed in ceramics derived from heated $Cs_{(1-x)}Na_xGPs$ when $x \leq 0.3$, as shown in **Figure 14**. It could be clearly observed that the particle size gradually

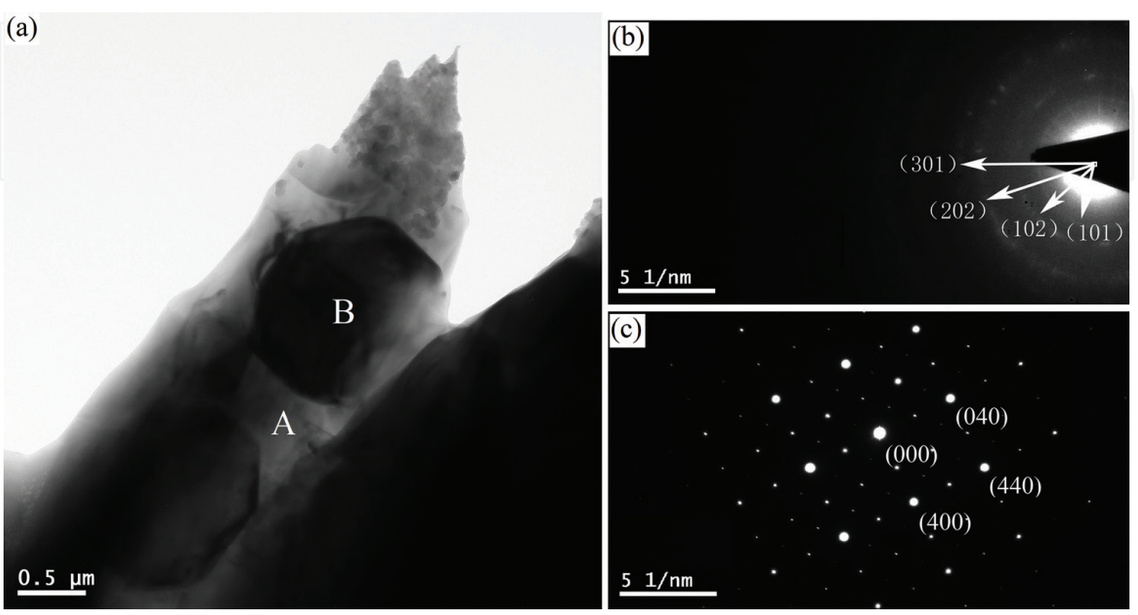

Figure 12.
TEM images of ceramics derived from $Cs_{(1-x)}Li_xGPs$, (a) x = 0.3, (b) and (c): SAED patterns of point A and B, respectively.

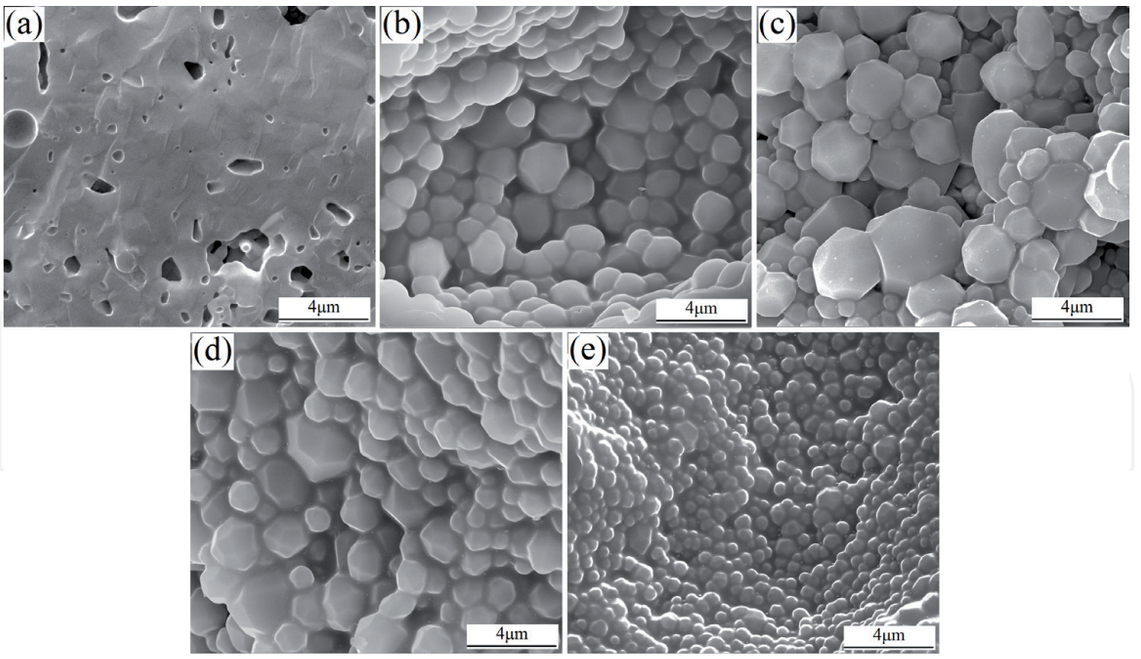

Figure 13.
Microstructure of ceramics derived from $Cs_{(1-x)}Na_xGPs$, (a) x = 0, (b) x = 0.1, (c) x = 0.2, (d) x = 0.3, (e) x = 0.4.

decreased with increasing Na^+ ion substitution. Compared with ceramics derived from pure CsGP, many pores could be observed, which should be attributed to the dissolution of the amorphous glass phase in the process of static etching. Due to the content of amorphous glass phase and the Na^+ ion substitution showed a proportional relationship. So, the residual amorphous glass phase will be more in the sample contained a higher Na^+ ion substitution. Take $Cs_{0.6}Na_{0.4}GPs$ for example, the vast majority of pollucite grains could not be observed clearly on the corroded surface of corresponding ceramic products due to the higher content of amorphous glass phase.

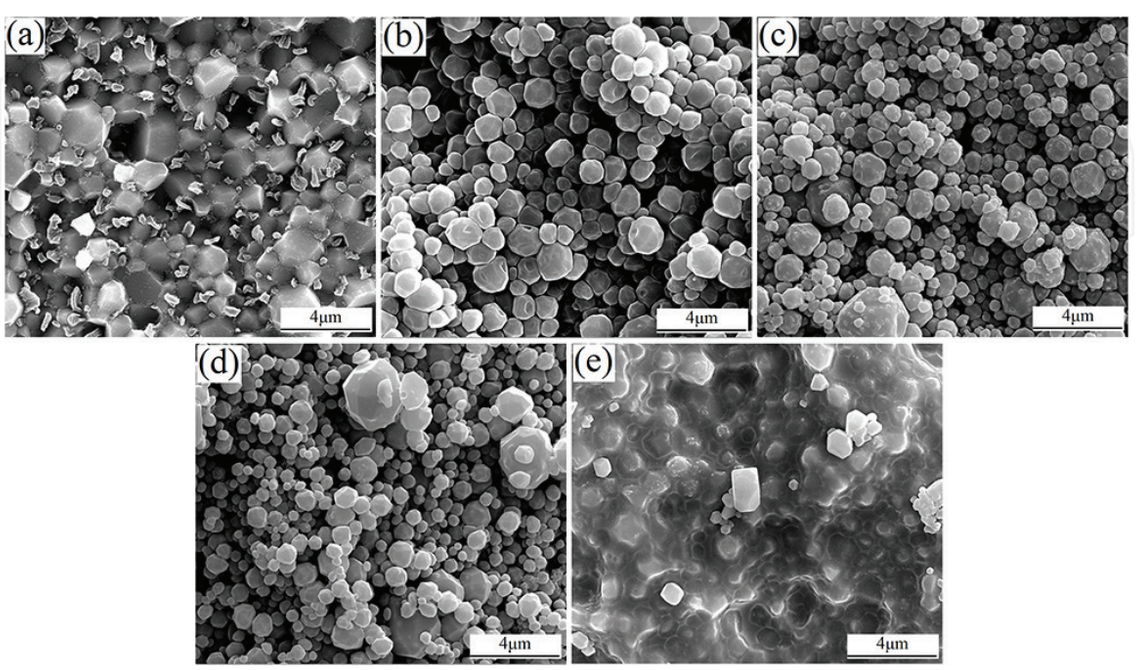

Figure 14.
Microstructure of ceramics derived from $Cs_{(1-x)}Na_xGPs$, (a) x = 0, (b) x = 0.1, (c) x = 0.2, (d) x = 0.3, (e) x = 0.4 etched in 4 wt% HF at room temperature for 20 s.

Figure 15 shows the TEM analysis of the ceramic evolved from treated $Cs_{0.6}Na_{0.4}GP$. Similar to $Cs_{(1-x)}Li_xGPs$ system, the presence of crystal grains could be clearly observed in this diphase composition system. The SAED patterns of area A (**Figure 15b**) suggested the crystal grain to be pollucite. The results of the map-scan suggested that Cs^+ ions were distributed only in the interior of crystal grain, which is consistent with the TEM results, as shown in **Figure 16**. However, Na^+ showed a completely different distribution. Map-scan results revealed that although the vast majority of Na^+ distributed among pollucite grains, there was still a small portion present in the interior of pollucite grains, which further demonstrated that Na^+ ions partially occupied Cs crystallographic sites of the pollucite framework during high-temperature processing. Combining the SAED patterns of area B (**Figure 15c**) and the result of the map-scan indicated again that the Na^+ ion mainly existed in the form of amorphous glass phase and distributed among the pollucite grains.

In heated $Cs_{(1-x)}Li_xGPs$ system, the particle size of pollucite coarsened with increases in Li substitution. However, $Cs_{(1-x)}Na_xGPs$ system showed a distinctly different variation tendency, in which the particle size of pollucite grains gradually decreased with increasing Na^+ ion substitution. The phenomenon of grain refinement in heated $Cs_{(1-x)}Na_xGPs$ system may have a direct relationship with the presence of zeolite nucleus in corresponding unheated samples. The zeolite nucleus formed in the unheated $Cs_{(1-x)}Na_xGP$ samples could serve as the nucleation site of pollucite and accelerate the crystallization process of pollucite. As already mentioned, the number of zeolite nucleus was proportional to Na^+ ion introduction. Therefore, the growth of pollucite grains was more dispersed as the nucleation sites increased.

3.4 Sintering mechanism

A possible sintering mechanism of $Cs_{(1-x)}Li_xGP$ system can be suggested in light of the theory of reactive liquid-phase sintering [46]. The composition of

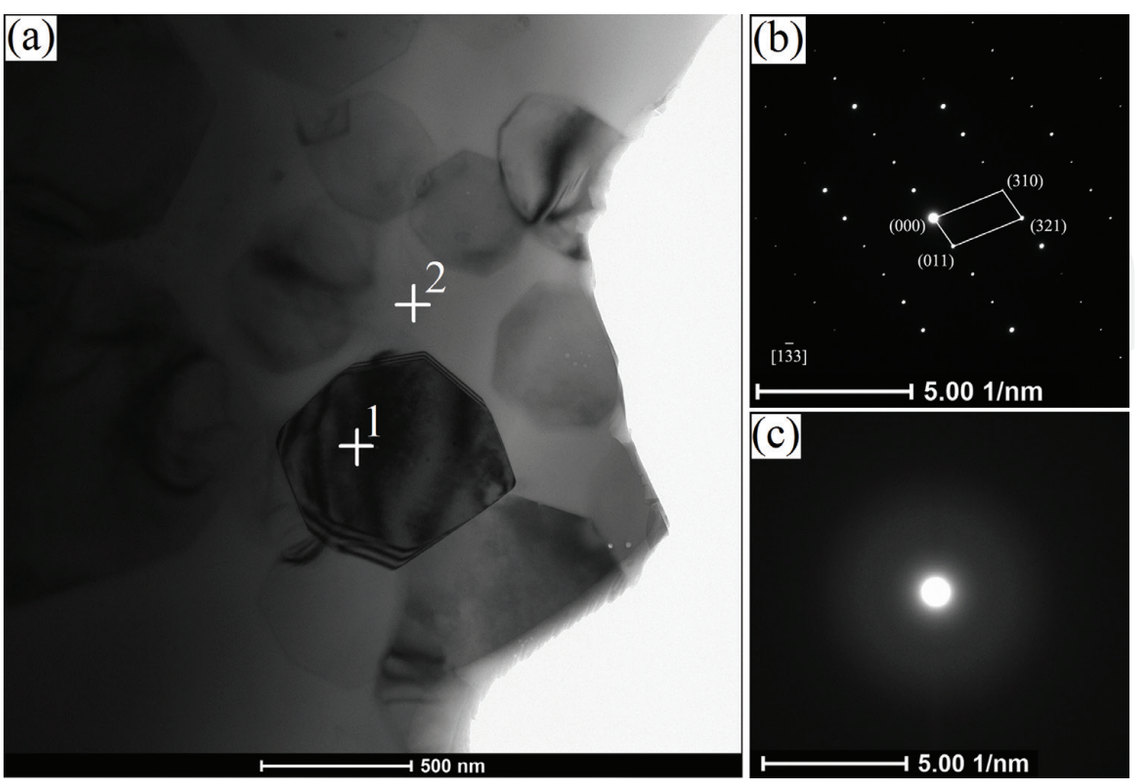

Figure 15.
TEM images of ceramics derived from $Cs_{(1-x)}Na_xGPs$, (a) x = 0.4, (b) and (c): SAED patterns of point 1 and 2, respectively.

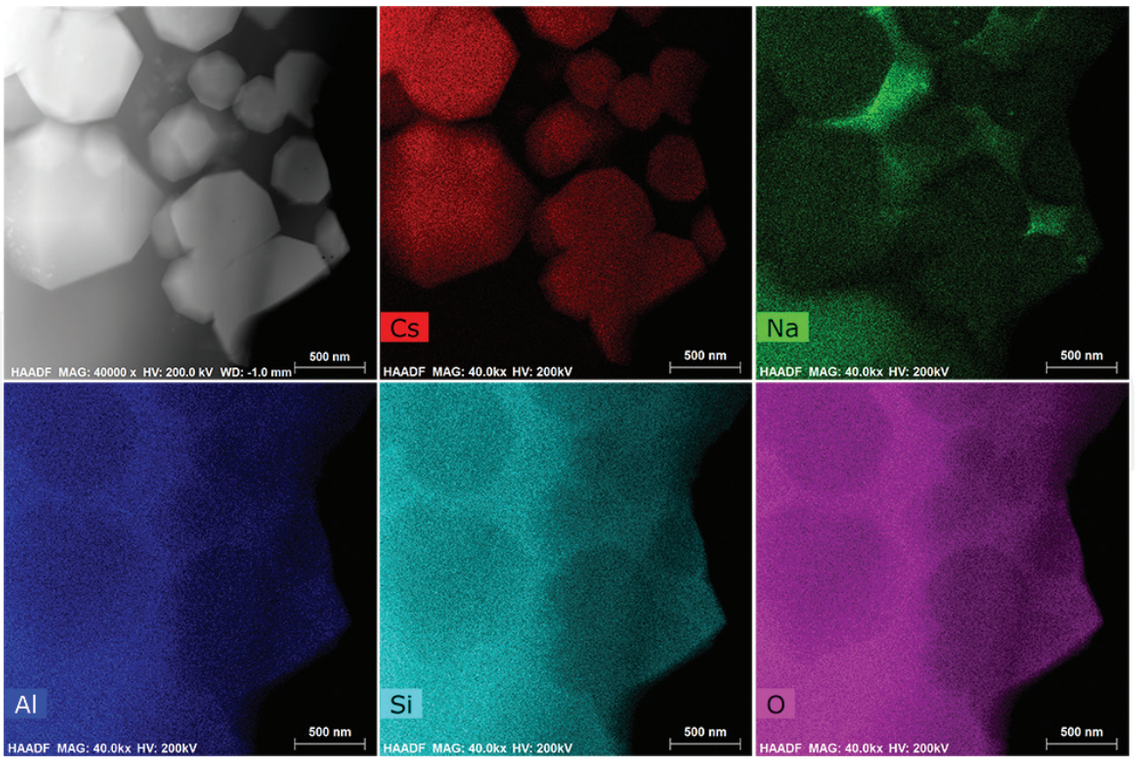

Figure 16.
HAADF-STEM and STEM-EDX images illustrating the element distribution.

$Cs_{(1-x)}Li_xGP$ can be expressed as $(1\text{-}x)Cs_2O{\cdot}xLi_2O{\cdot}Al_2O_3{\cdot}4SiO_2{\cdot}wH_2O$. In fact, both Li^+ and Cs^+ ions were present as silicates, that is, $x_1Li_2O{\cdot}y_1SiO_2$ and $x_2Cs_2O{\cdot}y_2SiO_2$ (the complexity of composition and structure of silicate indicated that x_1, y_1, x_2, and y_2 did not have a certain value). Therefore, it was reasonable to employ Li_2O and Cs_2O to express the form of Li^+ and Cs^+ ions in this system.

It well known that alkaline metal oxides often participated in the sintering process as a sintering aid in many low-temperature sintering systems [46, 47]. In addition, as a typical network-modifying agent, the presence of Li_2O or Li^+ ion could promote the densification process of sintering [48–51]. Similarly, the reaction between the alkaline metal oxide dopant and the matrix phase was studied and results showed that the mechanism was exactly the same in many cases. Hence, as for the $Cs_{(1-x)}Li_xGP$ system, Li^+ was an intermediate cation with a stronger electric field intensity in the glass-ceramic system than that of Cs^+ ion [52]. Thus, with increases in temperature of high-temperature processing, the reaction between Li_2O, Al_2O_3, and SiO_2 first occurred at a lower temperature, as in Eq. (1).

$$Li_2O(s) + SiO_2(s) + Al_2O_3(s) \rightarrow LiAlSi_2O_6(l) \quad (1)$$

The presence of liquid spodumene ($LiAlSi_2O_6$) and the simultaneous reaction between Li_2O and the matrix phase decreased the viscosity of the geopolymer system, which doubtlessly accelerated the kinetics of mass-transport processes during the low-temperature sintering. The changes in the sintering processes could reflect from the variation tendency in thermal shrinkage curves with different lithium contents (**Figure 3**). As the processing temperature rose further, the reaction between Cs_2O, Al_2O_3, and SiO_2 would occur at a higher temperature compared with the onset temperature of spodumene, as in Eq. (2).

$$Cs_2O(s) + SiO_2(s) + Al_2O_3(s) \rightarrow CsAlSi_2O_6(s) \quad (2)$$

The presence of liquid spodumene increased the rates of mass transfer and diffusion more easily, conducive to nucleation and crystallization of pollucite ($CsAlSi_2O_6$). This was consistent with the decrease in crystallization temperature and the grain coarsening behavior observed above with increasing lithium substitution. Meanwhile, the degree of densification was greatly improved as well. Therefore, the presence of Li^+ ion contributed to the crystallization and sintering densification via aiding the liquid-phase processes.

The sintering process of the $Cs_{(1-x)}Na_xGP$ system was similar to that of the $Cs_{(1-x)}Li_xGP$ system. The results above have already proved that $Cs_{(1-x)}Na_xGP$ ceramics only contained pollucite and amorphous glass phase. Therefore, the main difference in the sintering process between $Cs_{(1-x)}Li_xGP$ and $Cs_{(1-x)}Na_xGP$ systems lied in the low-temperature area. The reaction between Na_2O, Al_2O_3, and SiO_2 in the $Cs_{(1-x)}Na_xGP$ system would occur first at a lower temperature, as in Eq. (3).

$$Na_2O(s) + SiO_2(s) + Al_2O_3(s) \rightarrow \text{amorphous glass } (l) \tag{3}$$

In addition to this lower temperature, the sintering process of the two systems also experienced almost the same process at higher temperature intervals.

3.5 Thermal expansion behavior

The results of the dilatometric measurement for $Cs_{(1-x)}Li_xGP$ and $Cs_{(1-x)}Na_xGP$ ceramics with correction are shown in **Figure 17**. The thermal expansion of ceramics derived from $Cs_{(1-x)}Li_xGP$ and $Cs_{(1-x)}Na_xGP$ systems showed an increasing trend with increase in temperature, which could be attributed to the larger atomic spacing at elevated temperatures.

The average thermal expansion coefficient (CTE) was defined as the average value of the relative length change in the temperature range of $T_1 < T < T_2$, as described by the following Eq. (4):

$$\alpha_a = (L_2 - L_1)/L_0\ (T_2 - T_1) = \Delta L/L_0\ \Delta T \tag{4}$$

where L_0, L_1, and L_2 are the lengths of the specimen at temperatures of T_0 (30°C), T_1, and T_2, respectively. From **Figure 14**, both curves have two very different slopes before and after ~150°C, indicating that there was a phase transition for pollucite from tetragonal to cubic [24, 25]. Thus, the average CTE of $Cs_{(1-x)}Li_xGPs$ was computed based on data in the interval from 150 to 900°C.

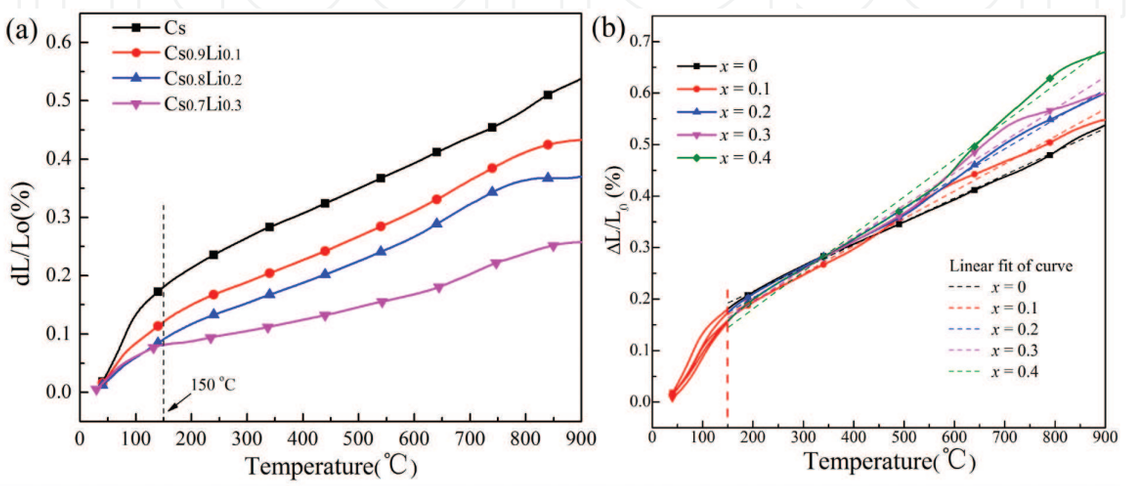

Figure 17.
Linear coefficient of thermal expansion of $Cs_{(1-x)}Li_xGP$ (a) and $Cs_{(1-x)}Na_xGP$.

As for $Cs_{(1-x)}Li_xGP$ ceramics, as depicted in **Figure 18**, it could be observed that the average CTE decreased from 4.80×10^{-6} K^{-1} ($x = 0$) to 3.61×10^{-6} K^{-1} ($x = 0.3$). The results obtained from our previous study on the $K_{(1-x)}Cs_xGP$ system proved that increase in Cs^+ ion introduction would decrease the average CTE of the resulting leucite ceramic. The reason could be attributed to the substitution between Cs^+ and K^+ in the leucite framework [33]. However, as for $Cs_{(1-x)}Li_xGP$ ceramics, the XRD results indicated almost no changes in lattice constants of pollucite, which suggested that the integrity of pollucite crystal cell was unchanged after partial substitution by Li^+ ion. XRD quantitative analysis suggested that the content of spodumene in resulting ceramic products was proportional to the amount of Li^+ ion substitution. By comparison, spodumene had a lower CTE (1.0×10^{-6} K^{-1}) than that of pollucite. Therefore, the presence of spodumene could significantly reduce CTE of the whole system, and the higher content of spodumene meant lower CTE. Another reason could be attributed to the role of molten spodumene, possibly as a buffer phase exists between pollucite crystals. Hence, with the increase in Li substitution or spodumene content, the average CTE of $Cs_{(1-x)}Li_xGP$ ceramics decreased evidently.

However, the calculated results showed that the average CTE of $Cs_{(1-x)}Na_xGP$ ceramic products showed a completely different variation pattern compared with $Cs_{(1-x)}Li_xGP$ ceramic products, increasing from 4.80×10^{-6} K^{-1} ($x = 0$) to 7.26×10^{-6} K^{-1} ($x = 0.4$) with the rise of sodium substitution.

For $K_{(1-x)}Cs_xGPs$ system involved in our previous studies, the average CTE of the leucite ceramic decreased with increase in the amount of Cs^+ ion introduced. The reason could be ascribed to Cs^+ occupying/substituting K^+ crystallographic sites in the leucite framework, which led to the increase in content of stabilized cubic leucite in resulting ceramic products [33]. However, there was no evidence to suggest any substitution at the lattice level between Li^+ and Cs^+ in the $Cs_{(1-x)}Li_xGP$ system. Besides, as a diphase system, pollucite and spodumene were present as independent components in the resulting products [38]. Therefore, one could conclude that the decline of average CTE was mainly due to the fact that CTE of spodumene was far lower than that of pollucite.

As for $Cs_{(1-x)}Na_xGP$ ceramics, XRD results suggested that the substitution between Na^+ and Cs^+ ions caused the decline of lattice constant of pollucite. According to the Ikuo et al. reports, the increase in Na^+ in the crystal lattice could decrease the thermal expansion of the pollucite, and with the increase in Na^+ ion substitution, the average CTE of ceramics derived from heated $Cs_{(1-x)}Na_xGPs$ decreased [24–26]. However, compared with $Cs_{(1-x)}Li_xGPs$ system, the CTE of $Cs_{(1-x)}Na_xGP$ ceramics showed an opposite trend with increasing Na^+ ion

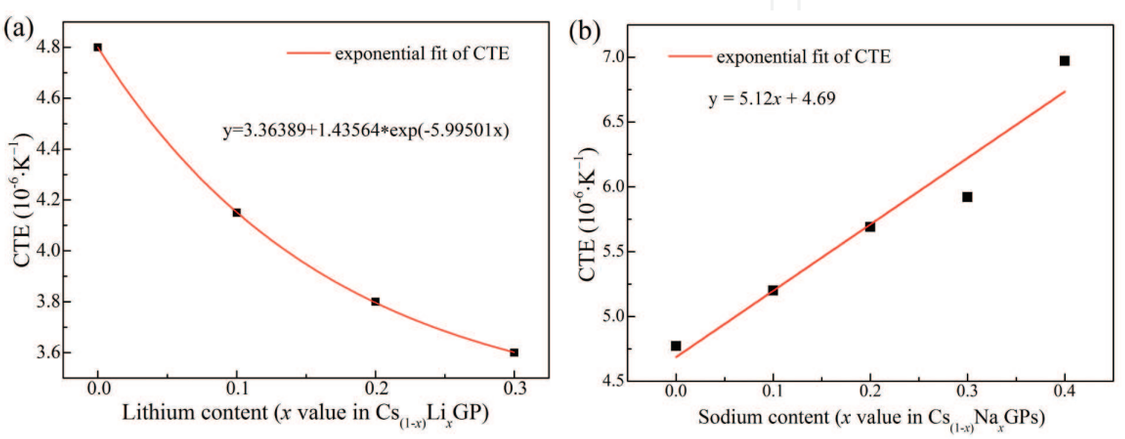

Figure 18.
Thermal expansion properties of $Cs_{(1-x)}Li_xGP$ ceramics (a) and $Cs_{(1-x)}Na_xGP$ ceramics (b).

substitution. The average CTE of $Cs_{(1-x)}Na_xGP$ ceramics continued to rise with the increase in content of Na^+ ion introduction. It is well known that amorphous glass phase containing Na^+ ion always had a higher CTE ($9\sim10 \times 10^{-6}\ K^{-1}$) than that of pollucite ($\sim4.80 \times 10^{-6}\ K^{-1}$) [53–56]. By contrast, the effect on CTE caused by the presence of the amorphous glass phase was much stronger than the impact caused by the substitution of Na^+ for Cs^+ in lattice level. So, the presence of amorphous glass phase could account for the rise of average CTE. The content of amorphous glass phase was proportional to the amount of Na^+ ion substitution. Therefore, the average CTE of ceramics derived from $Cs_{(1-x)}Na_xGPs$ increased almost linearly with the increasing sodium content.

4. Conclusions

In this chapter, the effects of ion substitution on the thermal evolution of cesium-based geopolymers on heating were studied. The following conclusions could be obtained based on the current results.

i. The introduction of Li^+ or Na^+ could favor the formation of pollucite in $Cs_{(1-x)}M_xGPs$ ($x \geq 0.1$), respectively. A possible reason could be attributed to the formation of zeolite nucleus, which could serve as the nucleation sites for pollucite. This also provided a novel method for preparing pollucite at low temperature, even at room temperature.

ii. $Cs_{(1-x)}M_xGPs$ with different content of ionic replacement showed a similar thermal evolution process. The introduction of Li^+ or Na^+ changed the sintering mechanism through decreased onset temperature for viscous sintering stage. With the introduction of more Li^+ or Na^+, the amorphous glass phase in resulting products would be conducive to its densification process. The introduction of Li^+ ion led to particle coarsening in part because of the rapid formation of a liquid phase on heating and perhaps because the hydration energy of Li^+ is greater than that of Cs^+. However, the particle size of pollucite grain gradually decreased with the increase in Na^+ contents in $Cs_{(1-x)}Na_xGP$ ceramics, which had a close relationship with the role of Na^+ ion in the nucleation process of pollucite.

iii. Compared with traditional way, geopolymer technology could be an excellent alternative to fabricate ceramics or ceramic matrix composites in an in-situ convert way. In the $Cs_{(1-x)}Li_xGP$ ceramics, the introduction of Li^+ results in the formation of a multiphase system, including pollucite, spodumene, and amorphous glass phase, and Li^+ only existed inside the spodumene grains. In contrast, two forms of Na^+ ions were present in the ceramic products derived from $Cs_{(1-x)}Na_xGPs$. Therefore, a small portion was present in the pollucite grains due to Na^+ occupying/substituting Cs^+ crystallographic sites of the pollucite framework, while the rest were mostly present in the amorphous glass phase and distributed among the pollucite grains.

iv. The average CTE of ceramics derived from $Cs_{(1-x)}Li_xGPs$ and $Cs_{(1-x)}Na_xGPs$ showed a completely different variation pattern. The reason could be attributed to the difference between two kinds of substituted ion species, which resulted in different phase composition in the corresponding resulting products.

Acknowledgements

The authors acknowledge the support from the National Natural Science Foundation of China (NSFC, Nos. 51372048, 51502052, 51321061 and 51225203). The grant from Fundamental Research Funds for the Central Universities (Grant no. HITNSRIF20165) is also acknowledged.

Author details

Jingkun Yuan[1*], Peigang He[1] and Dechang Jia[1,2]

1 Institute for Advanced Ceramics, School of Materials Science and Engineering, Harbin Institute of Technology, Harbin, Heilongjiang, China

2 State Key Laboratory of Advanced Welding and Joining, Harbin Institute of Technology, Harbin, Heilongjiang, China

*Address all correspondence to: yuanjingkun@126.com

References

[1] Hlaváček P et al. Inorganic foams made from alkali-activated fly ash: Mechanical, chemical and physical properties. Journal of the European Ceramic Society. 2015;**35**(2):703-709

[2] Favier A et al. Mechanical properties and compositional heterogeneities of fresh geopolymer pastes. Cement and Concrete Research. 2013;**48**:9-16

[3] Zhang Z, Yao X, Zhu H. Potential application of geopolymers as protection coatings for marine concrete I. Basic properties. Applied Clay Science. 2010;**49**(1-2):1-6

[4] Barbosa VFF, MacKenzie KJD. Thermal behaviour of inorganic geopolymers and composites derived from sodium polysialate. Materials Research Bulletin. 2003;**38**(2):319-331

[5] Slaty F et al. Durability of alkali activated cement produced from kaolinitic clay. Applied Clay Science. 2015;**104**(0):229-237

[6] Rickard W, Vickers L, van Riessen A. Performance of fibre reinforced, low density metakaolin geopolymers under simulated fire conditions. Applied Clay Science. 2013;**73**:71-77

[7] Temuujin J et al. Fly ash based geopolymer thin coatings on metal substrates and its thermal evaluation. Journal of Hazardous Materials. 2010;**180**(1-3):748-752

[8] Abdollahnejad Z et al. Mix design, properties and cost analysis of fly ash-based geopolymer foam. Construction and Building Materials. 2015;**80**:18-30

[9] Rahier H et al. Reaction mechanism, kinetics and high temperature transformations of geopolymers. Journal of Materials Science. 2006;**42**(9):2982-2996

[10] Messina et al. Alkali activated waste fly ash as sustainable composite: Influence of curing and pozzolanic admixtures on the early-age physico-mechanical properties and residual strength after exposure at elevated temperature. Composites Part B-Engineering. 2018;**132**:161-169

[11] Huseien GF et al. Geopolymer mortars as sustainable repair material: A comprehensive review. Renewable & Sustainable Energy Reviews. 2017;**80**:54-74

[12] MacKenzie KJD et al. Formation of aluminosilicate geopolymers from 1:1 layer-lattice minerals pre-treated by various methods: A comparative study. Journal of Materials Science. 2007;**42**(12):4667-4674

[13] Bell JL, Driemeyer PE, Kriven WM. Formation of ceramics from metakaolin-based geopolymers: Part I—Cs-based geopolymer. Journal of the American Ceramic Society. 2009;**92**(1):1-8

[14] Bell JL, Driemeyer PE, Kriven WM. Formation of ceramics from metakaolin-based geopolymers. Part II: K-based geopolymer. Journal of the American Ceramic Society. 2009;**92**(3):607-615

[15] El-Naggar MR, Amin M. Impact of alkali cations on properties of metakaolin and metakaolin/slag geopolymers: Microstructures in relation to sorption of Cs-134 radionuclide. Journal of Hazardous Materials. 2018;**344**:913-924

[16] Rees CA et al. In situ ATR-FTIR study of the early stages of fly ash geopolymer gel formation. Langmuir. 2007;**23**(17):9076-9082

[17] Cundy CS, Cox PA. The hydrothermal synthesis of zeolites:

Precursors, intermediates and reaction mechanism. Microporous and Mesoporous Materials. 2005;**82**(1-2):1-78

[18] Brady PV, Walther JV. Controls on silicate dissolution rates in neutral and basic pH solutions at 25°C. Geochimica et Cosmochimica Acta. 1989;**53**(11):2823-2830

[19] Duxson P, Lukey GC, van Deventer JSJ. Thermal evolution of metakaolin geopolymers: Part 1—Physical evolution. Journal of Non-Crystalline Solids. 2006;**352**(52-54):5541-5555

[20] Fernández-Jiménez A, Palomo A. Composition and microstructure of alkali activated fly ash binder: Effect of the activator. Cement and Concrete Research. 2005;**35**(10):1984-1992

[21] Fernández-Jiménez A, Palomo A, Criado M. Microstructure development of alkali-activated fly ash cement: A descriptive model. Cement and Concrete Research. 2005;**35**(6):1204-1209

[22] Fernández-Jiménez A et al. "Metakaolin-slag-clinker blends". The Role of Na^+ or K^+ as alkaline activators of theses ternary blends. Journal of the American Ceramic Society. 2013;**96**(6):1991-1998

[23] Duxson P et al. K-39 NMR of free potassium in geopolymers. Industrial & Engineering Chemistry Research. 2006;**45**(26):9208-9210

[24] Ikuo Y, Sachiko T, Hidehiko K. Low-thermal-expansion properties of sodium- and lithium-substituted cubic cesium leucite compounds. Journal of the American Ceramic Society. 2003;**86**(8):1360-1364

[25] Yanase I, Ichiyoshi K, Kobayashi H. Structural phase transition of Na-substituted Cs-leucite compounds in the range 123-1173 K. Solid State Communications. 2006;**139**(1):1-4

[26] Kobayashi H et al. Phase transition and lattice thermal expansion of cs-deficient pollucite, $Cs_{1-x}Al_{1-x}Si_{2+x}O_6$ ($x \leq 0.25$), compounds. Journal of the American Ceramic Society. 2006;**89**(10):3157-3161

[27] Yanase I, Konakawa J, Kobayashi H. Influence of cesium nitrate and heating rate on densification and microstructure of Cs-deficient pollucite sintered body. Journal of the American Ceramic Society. 2006;**89**(1):184-188

[28] Yanase I et al. Fabrication of low thermal expansion porous body of cubic cesium-deficient type pollucite. Journal of the European Ceramic Society. 2005;**25**(13):3173-3179

[29] Yanase I et al. Tetragonal-to-cubic structural phase transition in pollucite by low-temperature X-ray powder diffraction. Journal of the American Ceramic Society. 1997;**80**(10):2693-2695

[30] Yanase I, Kobayashi H, Mitamura T. Thermal expansion property of synthetic cubic leucite-type compounds. Journal of the Ceramic Society of Japan. 2000;**108**(1):26-31

[31] Yanase I, Kobayashi H, Mitamura T. Thermal property and phase transition of the synthesized new cubic leucite-type compounds. Journal of Thermal Analysis and Calorimetry. 1999;**57**(3):695-705

[32] Yanase I, Ishikawa Y, Kobayashi H. Effect of ball-milling on porous structure of Ca-substituted leucite porous body with low thermal expansion coefficient. Journal of the Ceramic Society of Japan. 2006;**114**(1336):1115-1120

[33] He P et al. Effect of cesium substitution on the thermal evolution

and ceramics formation of potassium-based geopolymer. Ceramics International. 2010;**36**(8):2395-2400

[34] He P, Jia D. Low-temperature sintered pollucite ceramic from geopolymer precursor using synthetic metakaolin. Journal of Materials Science. 2012;**48**(4):1812-1818

[35] Ranjbar N et al. Hot-pressed geopolymer. Cement and Concrete Research. 2017;**100**:14-22

[36] Duxson P, Lukey GC, van Deventer JSJ. Physical evolution of Na-geopolymer derived from metakaolin up to 1000°C. Journal of Materials Science. 2007;**42**(9):3044-3054

[37] Colic M et al. Effect of counterion size on short range repulsive forces at high ionic strengths. Langmuir. 1997;**13**(12):3129-3135

[38] Yuan J et al. Effects of Li substitution on the microstructure and thermal expansion behavior of pollucite derived from geopolymer. Journal of the American Ceramic Society. 2016;**99**(11):3784-3791

[39] Zhang M et al. A multiscale investigation of reaction kinetics, phase formation, and mechanical properties of metakaolin geopolymers. Cement & Concrete Composites. 2017;**78**:21-32

[40] Duxson P, Lukey GC, van Deventer JSJ. Evolution of gel structure during thermal processing of Na-geopolymer gels. Langmuir. 2006;**22**(21):8750-8757

[41] Duxson P, Lukey GC, van Deventer JSJ. The thermal evolution of metakaolin geopolymers: Part 2—Phase stability and structural development. Journal of Non-Crystalline Solids. 2007;**353**(22-23):2186-2200

[42] He Y et al. The hydrothermal transformation of solid geopolymers into zeolites. Microporous and Mesoporous Materials. 2012;**161**:187-192

[43] Qiu S et al. Strategies for the synthesis of large zeolite single crystals. Microporous and Mesoporous Materials. 1998;**21**(4):245-251

[44] Chlique C et al. XRD analysis of the role of cesium in sodium-based geopolymer. Journal of the American Ceramic Society. 2015;**98**(4):1308-1313

[45] Xie N, Bell JL, Krivenw WM. Fabrication of structural leucite glass-ceramics from potassium-based geopolymer precursors. Journal of the American Ceramic Society. 2010;**93**(9):2644-2649

[46] Valant M et al. A mechanism for low-temperature sintering. Journal of the European Ceramic Society. 2006;**26**(13):2777-2783

[47] Huang YR et al. Lithium aluminosilicate glass-ceramic containing Na_2O for low-temperature anodic bonding in microelectronic mechanical systems. Journal of Non-Crystalline Solids. 2008;**354**(12-13):1407-1410

[48] Goharian P et al. Lithium ion-conducting glass-ceramics in the system Li_2O-TiO_2-P_2O_5-Cr_2O_3-SiO_2. Journal of Non-Crystalline Solids. 2015;**409**:120-125

[49] He LT, Xia GB, Yang DA. Synthesis and characterization of LTCC composites based on the spodumene/anorthite crystallizable glass. Journal of Alloys and Compounds. 2013;**556**:12-19

[50] Ding YJ et al. Influence of alkali metal compound fluxes on Gd_2O_2S:Tb particle and luminescence. Journal of Materials Science: Materials in Electronics. 2015;**26**(3):1982-1986

[51] Miller MJ, Wang JL. Influence of Na diffusion on thermochromism of

vanadium oxide films and suppression through mixed-alkali effect. Materials Science & Engineering, B: Advanced Functional Solid-State Materials. 2015;**200**:50-58

[52] Cai DL et al. Inhibiting crystallization mechanism of h-BN on alpha-cordierite in BN-MAS composites. Journal of the European Ceramic Society. 2016;**36**(3):905-909

[53] Thieme C, Ruessel C. High thermal expansion of crystallized glasses in the system BaO-ZnO-NiO-SiO_2. Ceramics International. 2015;**41**(10):13310-13319

[54] Utracki LA. Compressibility and thermal expansion coefficients of nanocomposites with amorphous and crystalline polymer matrix. European Polymer Journal. 2009;**45**(7):1891-1903

[55] Durandurdu M. Vibrational properties of amorphous germanium under pressure and its thermal expansion and Gruneisen parameters. Journal of Non-Crystalline Solids. 2010;**356**(20-22):977-981

[56] Som T, Karmakar B. Structure and properties of low-phonon antimony glasses and nano glass-ceramics in K_2O-B_2O_3-Sb_2O_3 system. Journal of Non-Crystalline Solids. 2010;**356**(20-22):987-999